Temperature-Dependent Change of the Electronic Structure in the Kondo Lattice System $YbRh_2Si_2$

Temperature-Dependent Change of the Electronic Structure in the Kondo Lattice System $YbRh_2Si_2$

S. Y. Agustsson,[1] S.V. Chernov,[1] K. Medjanik,[1] S. Babenkov,[1] O. Fedchenko,[1] D. Vasilyev,[1] C. Schlueter,[2] A. Gloskovskii,[2] Yu. Matveyev,[2] K. Kliemt,[3] C. Krellner,[3] J. Demsar,[1] G. Schönhense,[1] and H.J. Elmers[1,*]

[1] *Institut für Physik, Johannes Gutenberg-Universität, Staudingerweg 7, 55128 Mainz, Germany*

[2] *Deutsches Elektronen-Synchrotron DESY, 22607 Hamburg, Germany*

[3] *Physikalisches Institut, Goethe Universität Frankfurt, Max-von-Laue-Strasse 1, 60438 Frankfurt am Main, Germany*

The heavy-fermion behavior in intermetallic compounds manifests itself in a quenching of local magnetic moments by developing Kondo spin-singlet many-body states combined with a drastic increase of the effective mass of conduction electrons, which occurs below the lattice Kondo temperature T_K. This behavior is caused by interactions between the strongly localized $4f$ electrons and itinerant electrons. A controversially discussed question in this context is how the localized electronic states contribute to the Fermi surface upon changing the temperature. One expects that hybridization between the local moments and the itinerant electrons leads to a transition from a small Fermi surface in a non-coherent regime at high temperatures to a large Fermi surface once the coherent Kondo lattice regime is realized below T_K. We demonstrate, using hard X-ray angle-resolved photoemission spectroscopy that the electronic structure of the prototypical heavy fermion compound $YbRh_2Si_2$ changes with temperature between 100 and 200 K, i.e. far above the Kondo temperature, $T_K = 25$ K, of this system. Our results suggest a transition from a small to a large Fermi surface with decreasing temperature. This result is inconsistent with the prediction of the dynamical mean-field periodic Anderson model and supports the idea of an independent energy scale governing the change of band dispersion.

I. INTRODUCTION

The low-temperature physics of strongly correlated electron systems is governed by electronic states near the Fermi surface and their interactions with other low energy excitations[1]. In contrast to superconductors, where the many-body electron correlation causes a gap, i.e. a depleted density of states, near the Fermi surface, Kondo systems reveal an increased density of states at the Fermi surface at low temperatures[2–4]. In this case, the interaction of localized moments and itinerant valence electrons results in a correlated state. This correlated state originates from the formation of Kondo singlets, where valence electrons screen localized magnetic moments. This screening occurs below a characteristic temperature, which is called the Kondo temperature. Similar to Cooper pairs the Kondo singlet states do not show up in the single particle density of states as measured by single-particle excitations. However, the hybridization of localized and itinerant states leads to the increased single-particle density of states[5].

In a translational symmetric lattice of local moments the Kondo coupling also leads to the formation of coherent quasi-particle states at the Fermi energy, being the analog of the Kondo resonance for a local magnetic impurity site[6]. In such a lattice not only the density of states at the Fermi surface is increased due to the Kondo effect but also the momentum dependence of the states reacts on the formation of correlated states and changes its topology[7]. Conduction electrons acquire a huge effective mass, which coined the name heavy fermion system. The localized f-electrons involved in the hybridization are then included in the Fermi surface encompassing all occupied states[6]. If the moments become unscreened, which may be provoked by a magnetically ordered state at very low temperatures or by lifting the coupling of conduction electrons with the local moments above the Kondo temperature, the underlying f-electrons become localized and are thus excluded from the Fermi surface. The Fermi surface is therefore increased in the Kondo lattice state with respect to the uncorrelated state. These two situations are also known as the large and small Fermi surfaces, respectively[8,9].

An unsolved question is at which temperature the transition from the large to the small Fermi surface occurs. At very low temperature the occurrence of an antiferromagnetic order in some Kondo lattices should quench the screening of localized moments. For the case of $YbRh_2Si_2$ one expects this to happen below the Néel temperature of 70 mK. On the other

hand, the large Fermi surface should also become small at temperatures above the Kondo temperature of $T_K = 25$ K, associated with the loss of coherence of the heavy fermion quasiparticles. Indeed, the periodic Anderson model predicts the loss of coherence in close proximity to T_K[10]. In contrast, dynamical mean-field theory calculations predict a continuous change of the Fermi surface above T_K[11]. Angle-resolved photoemission spectroscopy (ARPES) on $YbRh_2Si_2$ provides a direct experimental access to the Fermi surface[8,12–14], revealing a temperature-independent Fermi surface in a wide temperature range between 1 and 100 K[15].

Coherence loss and change of band structure are likely different properties[16]. In $YbRh_2Si_2$ coherence sets in below 100 K as observed in resistivity[17], while the formation of the $4f$-derived flat band sets in at temperatures above 120 K, as seen by spectroscopic features in scanning tunneling spectroscopy[18] and ARPES[19]. Thus, the current picture is that starting from room temperature the $4f$-derived bands form already at higher temperature, while coherence sets in when the higher crystalline electric field induced levels are depopulated and only the ground state is occupied[18].

Up to now, experimental evidence for the large-to-small Fermi surface transition in heavy fermion systems[20–23] and for the suppression of the Kondo state[24] with increasing temperature is still weak and indirect. Recently, technological advances of hard X-ray sources and photoelectron detectors[25–28] enabled high energy angle-resolved photoemission spectroscopy for bulk states of complex compounds. In this article, we demonstrate strong indication of temperature-induced changes of the Fermi surface in $YbRh_2Si_2$ accompanied by changes of the band dispersion in the temperature range between 100 and 300 K, i.e., across the high-temperature (single impurity) Kondo energy scale.

II. METHOD

Single crystals of the heavy fermion compound $YbRh_2Si_2$ have been fabricated using a high-temperature indium-flux technique as described in Ref.[29]. The single crystals were glued using epoxy resin onto the sample holder with the (001) plane parallel to the sample holder plate. Prior to the transfer into the vacuum chamber, the crystals were cleaved using a wire cutter. The samples are inserted into a He-cooled (20 K) sample stage on a high precision 6-axis hexapod manipulator of the time-of-flight momentum microscope.

The experiments have been performed at beamline P22 of the storage ring PETRA III at DESY in Hamburg (Germany). Owing to the high energy (6.0 GeV) and large size (2.3 km circumference) of PETRA, P22 provides hard X-rays with the highest brilliance worldwide in an energy range from 2.4 to 15 keV. Present conditions were 2×10^{13} photons/s at 5.297 keV in a spot of about 10×10 μm^2 using a Si(311) double-crystal monochromator[27]. At 5.297 keV the overall energy resolution is determined by the photon band width of 155 meV.

A key benefit of angle-resolved photoelectron spectroscopy in the hard X-ray range is the significant increase of the inelastic mean free path of the escaping photoelectrons[25,30,31]. Therefore, the present results represent true bulk properties.

To resolve the challenge of low cross section and low signal-to-background ratio in the hard X-ray regime we applied time-of-flight momentum microscopy[28], allowing for high-efficiency 3-dimensional data acquisition of the photoelectron intensity $I(E_B, k_x, k_y)$ as a function of binding energy, E_B, and momentum. The large momentum field of view of 12 Å^{-1} simultaneously yields five adjacent Brillouin zones, where larger parallel momentum results in decreasing perpendicular momentum. This allows us to resolve the perpendicular momentum k_z, covering a range of $\Delta k_z = 0.5 G_{001}$ in one experimental run, The parallel momentum resolution of the instrument depends on the field of view. For the large k-fields of 12 Å^{-1} in diameter we estimate a resolution of 0.04 Å^{-1}. Data processing for noise suppression limits the resolution to 0.08 Å^{-1} for the results presented in the following.

Data have been acquired at 20 K and 300 K for 8 hours in each case. During cooling, data acquisition at four intermediate temperatures has been limited to 30 minutes in each case. Details of the data evaluation procedure have been described in Refs.[26,27].

III. RESULTS

The Fermi surface sum rule provides a fundamental principle for strongly correlated systems[6]. The sum rule states that the Fermi surface area is conserved in the presence of interactions as long as the interactions do not give rise to a phase transition. Thus, if the local orbital magnetic moments are quenched by the Kondo effect, the underlying localized electrons must be included in the conduction bands, whereas they are excluded from it in the unscreened state[9]. The corresponding changes of the electronic bands for $YbRh_2Si_2$ near the Fermi energy are sketched in Fig. 1. Fig. 1(a,b) shows the calculated

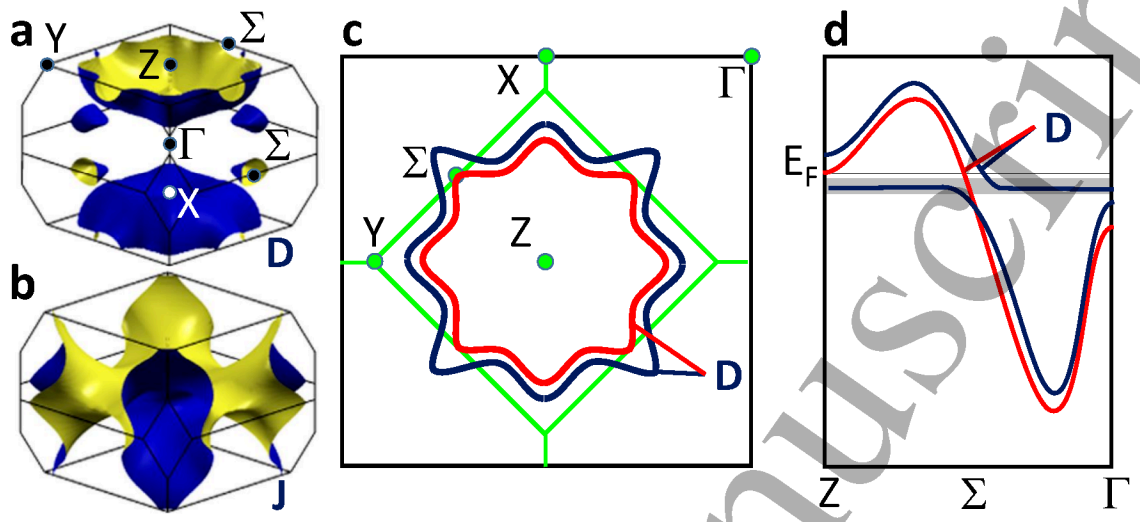

FIG. 1. (a) Calculated Fermi surface sheets D (Doughnut) and (b) J (Jungle Gym) for $YbRh_2Si_2$ according to Ref. 32. (c) Schematic representation of a cut through the Doughnut in the Z-Y-Σ plane for low temperature (blue) in the correlated state and for high temperature (red) without electron correlation. (d) Schematic band dispersion along the Z-Σ-Γ momentum direction for low (blue) and high (red) temperatures.

Fermi surface of $YbRh_2Si_2$ with the $ThCr_2Si_2$-structure type (space group I4/mmm) from Ref.[32]. The Fermi surface comprises two bands forming the compact Doughnut sheet D near the Z point [Fig. 1(a)] and the fractional Jungle-Gym sheet J [Fig. 1(b)]. The planar cut at the high symmetry plane Z-Σ-Y through band D for the cases of large and small Fermi surface is depicted in Fig. 1(c). The difference of the calculated Fermi wave vectors between the low and high temperature phases is larger along the Z-Σ direction as compared to the Z-Y direction. Fig. 1(d) illustrates how hybridization of the localized moment with the conduction band electrons enlarges the size of the hole-like Fermi surface. The hybridization with the localized states increases the Fermi wave vector along the Z-Σ direction by an upward bending of the band close to the crossing point of itinerant and localized states. In addition to the hybridization, the formation of Kondo states extracts itinerant electrons from the D band leading to a lower band filling, i.e. to a shift of the band to higher energy

with respect to the Fermi energy. If the strong coupling is released, the liberated electrons will fill the band and thus shift band D as depicted in Fig. 1(d) to lower energy with respect to the Fermi level.

First, we discuss the experimentally determined $YbRh_2Si_2$ bulk electronic structure in 3-dimensional momentum space. The photon energy of $h\nu = 5297$ eV results in $k_z = NG_{001}$, with an integer number N=29, assuming that the final state can be described by a free electron state[27]. Note that the photon momentum shifts the direction of normal emission away from the Γ point, corresponding to the initial state with momentum zero, by more than the size of one Brillouin zone. At the large photon energy of the present experiment, the change of the perpendicular momentum across the Brillouin zone section close to normal emission, i.e. with small parallel momentum, amounts to less than 0.05 $Å^{-1}$. This value is less than 0.06 G_{001}. We have neglected this variation and symmetrized the data from this Brillouin zone section according to the crystal symmetry with $I(k_x, k_y) = I(-k_x, k_y)$ and $I(k_x, k_y) = I(k_x, -k_y)$. The result represents a cut along the central Γ-X-Σ plane through the Brillouin zone. Compared to the high kinetic energy of several keV, a few eV binding energy do not notably change k_z. Accordingly, the dispersion of bands $E(k_x, k_y)$ along the parallel high symmetry directions through the Γ point is also captured by this procedure.

At hard X-ray energies the final states are predominantly of free-electron type and therefore the transition matrix elements vary to a lesser extent as compared to photon energies used in conventional ARPES. Consequently, the measured photoemission intensity $I(E_B, k_x, k_y, k_z)$ approximates the spectral density of states $\rho(E_B, k_x, k_y, k_z)$. Note, however, that $I(E_B, k_x, k_y, k_z)$ does not exactly represent the spectral density because of different cross sections for different orbital characters of the initial states.

Surfaces of constant energy in three-dimensional k-space result from cuts of the four-dimensional array $\rho(E_B, k_x, k_y, k_z)$. The cut for $E_B = 0$ then represents the Fermi surface. Note, that the cut of $\rho(E_B, k_x, k_y, k_z = NG_{001})$ not only covers the central Γ-X-Σ section but also the Z-Σ-Y plane of the Brillouin zone, due to the repeated Brillouin zone scheme in reciprocal space. The latter is divided into four triangles in the corners of the square that embraces the central Brillouin zone cut. The analogous situation for the Z point placed in the center of the square is shown in Fig. 1(c).

Due to the translational symmetry, we will discuss the results in the reduced zone scheme and obtain $\rho(E_B, k_x, k_y, k_z = NG_{001}) = \rho(E_B, k_x, k_y, k_z = 0)$. Exploiting the simultaneous

data acquisition of a large field-of-view, comprising more than 25 adjacent Brillouin zones, we derive similar cuts at different k_z values, $\rho(E_B, k_x, k_y, k_z = xG_{001})$, from Brillouin zones centered at larger parallel momentum. In the extended zone scheme the final-state sphere cuts different Brillouin zones in different sectional planes (for details, see Fig. 6 in Ref.[27]). With this procedure we determined 8 distinct cuts in the interval from $x = 0$ to $x = 0.5$. Note that the cuts near 0.25 G_{001} average over a larger k_z interval of 0.1 G_{001} due to the decreasing value of k_z with increasing parallel momentum. Thus, using the symmetry relation $\rho(E_B, k_x, k_y, k_z) = \rho(E_B, k_x, k_y, -k_z)$ we obtain data for the complete Brillouin zone from one data set taken at a single photon energy.

Fig. 2(a) shows the Fermi surface of $YbRh_2Si_2$ at 20 K in a three-dimensional color coded intensity map. The Doughnut (D) can be identified near the Z points. The Jungle Gym (J) surface appears fractionated due to the matrix element induced intensity variations. Figs. 2(b-d) depict the constant energy surfaces at higher binding energies. Due to the hole-like dispersion of bands D and J the spectral densities retract towards the Brillouin zone edges. At higher binding energy lower lying bands appear near the Z and X points (Fig. 2(d)).

For the discussion of correlation-induced changes of the band dispersion we focus on the square area of the Brillouin zone near the Z point, which has been previously identified as the decisive k-space section to address the question of variation from the small to the large Fermi surface[8,9]. The low temperature constant energy map shown in Fig. 3(a) reveals the cut through the band D (Doughnut) as schematically depicted in Fig. 1(a,c). Here, the Fermi surface extends beyond the first Brillouin zone along the Z-Σ direction. A higher spectral density, likely stemming from the so-called pill-box band[32], appears close to the Γ point in the corner of the map, which lies in the center of the adjacent Brillouin zone. At higher binding energy $E_B = 0.4$ eV [Fig. 3(b)] the high intensity near the Γ point has vanished. In this case, band D has an almost circular shape, indicating a reduced wave vector below the average $4f$ binding energy. Apparently, this happens despite the band dispersion being hole-like, i.e. with increasing wave vector for increasing binding energy. The hole-like dispersion of band D becomes obvious from the constant energy cuts at $E_B = 0.9$ eV and $E_B = 1.5$ V (Figs. 3(c,d)), where the D-band contour appears with increasing radius. Fig. 3(d) also indicates the appearance of a second band at 1.5 eV binding energy with a maximum at the Z-point.

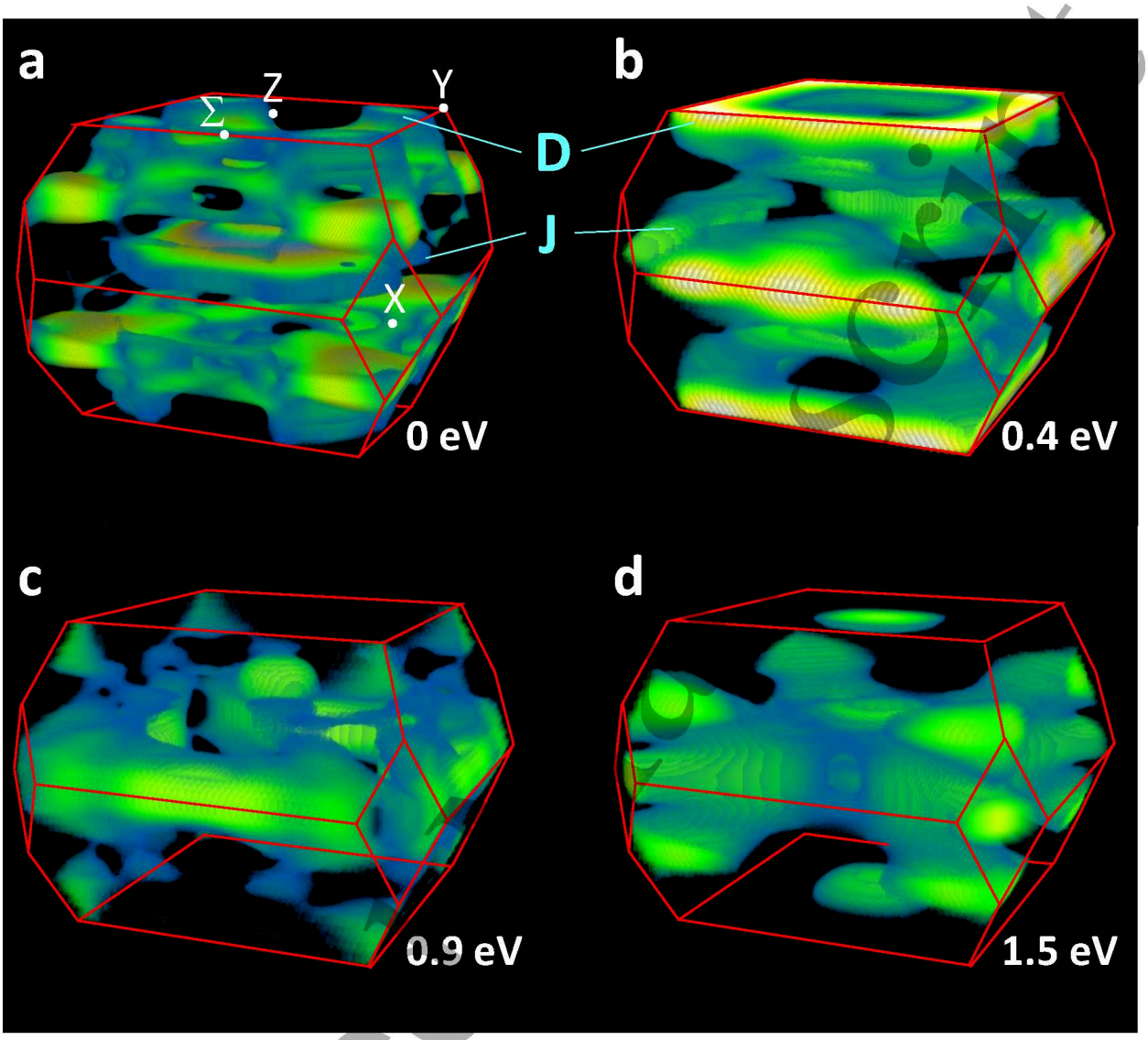

FIG. 2. (a) Three-dimensional representation of the measured spectral density of states of $YbRh_2Si_2$ at the Fermi level $\rho(E_B = 0, k_x, k_y, k_z)$ (Fermi surface) with indicated Brillouin zone and high-symmetry points extracted from hard X-ray photoemission excited by a photon energy of 5297eV at a temperature of 20 K. (b-d) Corresponding constant energy surfaces at binding energies $E_B = 0.4$ eV, 0.9 eV, and 1,5 eV.

The energy dispersions $E_B(k)$ of the bands are visualized by cuts along the high symmetry directions Z-Y and Z-Σ in Figs. 3(e,f). Here, the intensity has been normalized to the momentum-integrated intensity, $I_N(E_B, k_x, k_y) = I(E_B, k_x, k_y)/\int_{BZ} I(E_B, k_x, k_y)dk_x dk_y$. The normalization removes the variation of the photoemission intensity due to the localized 4f-states and due to quasi-elastic phonon scattering. This processing suppresses the high

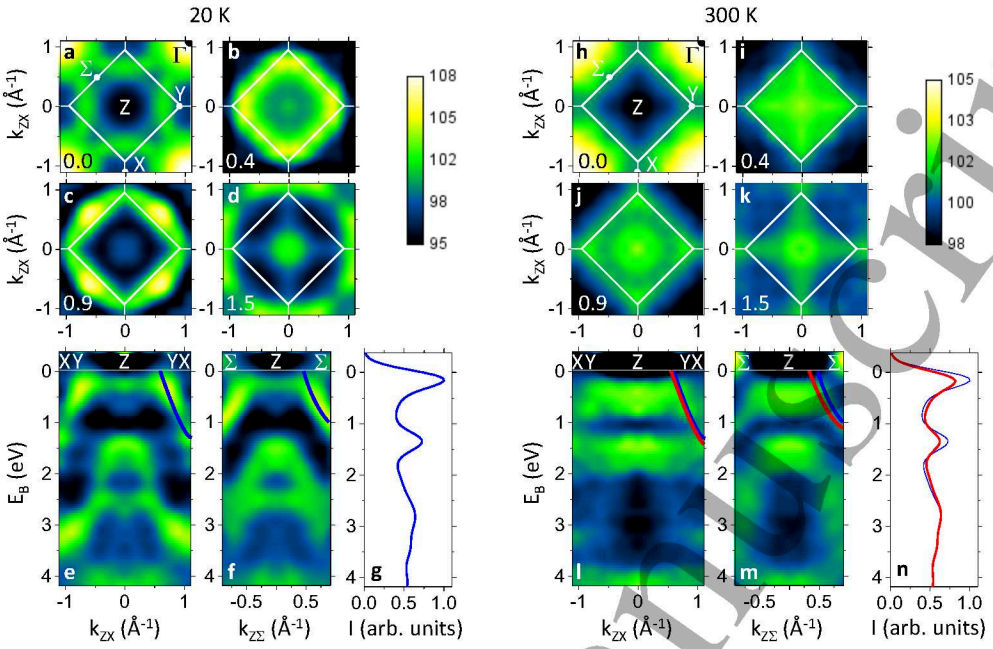

FIG. 3. (a) Constant-energy map of the spectral density of electronic states after re-normalization (see text) $\rho(E_B = 0, k_x, k_y, k_z = 0.5\ G_{001})$ in the Z-Y-Σ plane measured at 20 K. Note that the plane extends to the Γ-X-Σ plane of the adjacent Brillouin zones towards the corners of the image. (b-d) Corresponding constant energy maps at binding energies $E_B = 0.4$ eV, 0.9 eV, and 1.5 eV. (e) Energy dispersion along Z-Y and (f) along Z-Σ, respectively. The color code for (a-f) is indicated in the upper right panel. (g) Integrated spectral density (without normalization) representing the density of states versus binding energy. This data is used for the normalization processing in (e,f). (h-n) Analogous data obtained for 300 K.

momentum-independent intensity stemming from the localized $4f$ states. Thus, the normalization emphasizes the dispersion of electronic bands on the expense of suppressing the signal from the non-dispersive part of the localized $4f$-states

The corresponding color code (in percent of the average value) is shown to the right of Figs. 3(b,d). The remaining large momentum-independent background intensity, which is suppressed by the choice of the color code, is a result of quasi-elastic scattering of photoemitted electrons with phonons. Such scattering events almost conserve the kinetic energy of photoemitted electrons (maximum phonon energies are of the order of tens of meV), but randomize their momentum distribution. Due to this background intensity the signal, carry-

ing the information of electron momentum, presents only a few percent of the total acquired photoelectron intensity.

The solid blue lines shown in Figs. 3(e,f) for positive momentum values indicate the position and dispersion of band D at 20 K. Due to the finite energy resolution, the dispersion map does not capture the hybridization of band D with the Yb $4f$ states.

The integrated photoelectron intensity (here without normalization) is shown in Fig. 3(g), revealing two intensity maxima indicating the spin-orbit split Yb $4f$ states. Their splitting of 1.3 eV, smaller binding energy of $E_B = 0.15$ eV and their energy widths are in good agreement with earlier results[9,15].

The corresponding results obtained at 300 K are shown in Figs. 3(h-n). At high temperature the constant background intensity has significantly increased compared to the 20 K case due to the Debye-Waller factor[26]. This is accounted for by the different color map. Again, band dispersion can not be resolved within the energy interval covering the hybridization energy close to the Fermi energy. As a consequence, the Fermi surface map (Fig. 3(h)) does not clearly show the shape of the Doughnut section. The intensity maximum near the Γ point appears more pronounced compared to the low temperature data, shown in Fig. 3(a), revealing a decrease in energy of the corresponding electron-like band. At larger binding energy $E_B = 0.4$ eV (Fig. 3(i)) band D appears with a cross-like shape. Compared to the corresponding low-temperature data (Fig. 3(b)), the wave vector of band D is substantially reduced along the Z-Σ direction. This observation is supported also by the comparison of Figs. 3(c) and (j) for $E_B = 0.9$ eV. Here, the circular-shaped band D at 20 K is transformed into a square-like shape at 300 K.

The corresponding energy dispersion $E_B(k)$ of the bands visualized by cuts along the high symmetry directions Z-Y and Z-Σ in Figs. 3(l,m) reveal a similar behavior to the low-temperature data. A close inspection shows that band D is shifted at 300 K to higher binding energies. In order to emphasize this effect, the dispersion of the band is depicted by solid red lines in Figs. 3(l,m) in comparison to the low-temperature dispersion, indicated by blue lines in the same plots. The energy shift amounts to about 100 meV. Bands at larger binding energies $E_B(k) > 1$ eV are broadened due to the phonon scattering, yet they appear to be unchanged with respect to the 20 K data within the error bars.

The integrated photoelectron intensity (without normalization) shown in Fig. 3(n) is similar to the one measured at low temperature. The energetic position and spin-orbit

splitting of the Yb $4f$ states has not changed at 300 K. The density of states maximum near the Fermi level has slightly decreased at 300 K with respect to the average spectral density, which is in good agreement with earlier results[15].

For a more detailed analysis we discuss momentum distribution curves (MDC) along the Z - Σ direction. Raw data and the corresponding processed constant-energy maps utilizing Gaussian smoothing are shown in Figs. 4(a-d). We compare the MDCs at selected binding energies extracted from the raw and processed images at 20 K and 300 K in Figs. 4(e,f). At $E_B = 1.1$ eV one observes a maximum in intensity at ± 0.9 Å^{-1}. This maximum corresponds to band D, dispersing towards the Z point with decreasing binding energy. At 20 K the maximum lies at ± 0.8 Å^{-1} for a binding energy of 0.8 eV. The same maximum lies at ± 0.7 Å^{-1} at 300 K. At a binding energy of 0.5 eV, the maximum has dispersed at 20 K to ± 0.7 Å^{-1}. The same maximum lie at 300 K at ± 0.5 Å^{-1}. For a range of binding energies, the corresponding maxima lie at larger momentum values for 20 K as compared to 300 K. The momentum distribution curves reveal a significant difference of the band dispersion of band D between 20 K and 300 K in a binding energy range from $E_B = 0.4$ eV to 1.1 eV. This result suggests a shift of band D to higher binding energy for 300 K.

To gain further insight into the temperature-driven changes in the electronic structure, we compare MDCs in Fig. 5 as a function of temperature. To determine the temperature range, where the change from the large to the small Fermi surface occurs (using the changes in the D band as a fingerprint), we performed a series of measurements at intermediate temperatures while slowly cooling the sample. The momentum distribution curves along the Z - Σ direction reveal a significant variation with temperature between 200 K and 100 K as shown in Fig. 5. At $E_B = 0.4$ eV [Fig. 5(a)], the distance of the trailing edge of band D from the Z point, $K_{Z\Sigma}$, shows an increase of 0.15 Å^{-1} between 200 K and 100 K. Similarly, the momentum of the intensity maximum of band D increases from 0.55 Å^{-1} to 0.65 Å^{-1} with decreasing temperature.

Momentum distribution curves at the Fermi level ($E_B = 0$ eV) also suggest temperature induced changes at the Fermi surface [Fig. 5(b)]. Here, the intensity monotonously increases along the trace from Z over Σ to Γ for 300 K. In contrast, the intensity shows a plateau or even decreases at Σ for $T <= 100$ K. The 200 K data at the Fermi energy suffers from poor statistics. The comparison of results for 20 K and 300 K is compatible with a difference of the electronic structure at the Fermi level. For the data obtained at the Fermi level

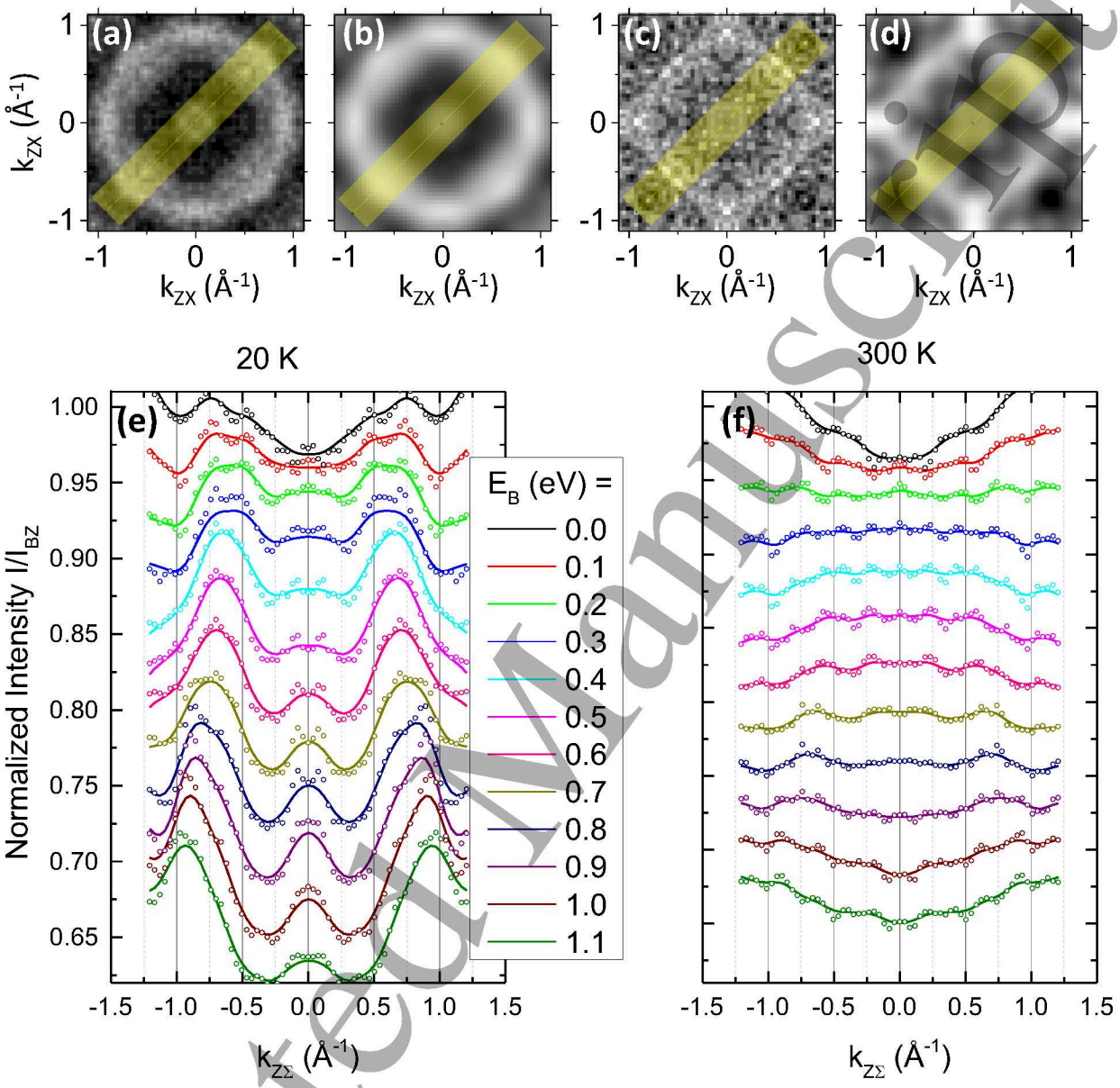

FIG. 4. (a,b) Constant-energy maps of the spectral density of electronic states after renormalization measured at 30 K; (a) raw data and (b) processed with a Gaussian smoothing with a radius of 0.08 Å^{-1} in momentum space. (c,d) Similar data measured at 300 K. (e,f) Momentum dispersion curves for indicated binding energies recorded at 20 K (e) and 300 K (f). Open circles are obtained from the raw data according to the yellow-shaded profile in (a,c). Solid lines are obtained from (b,d).

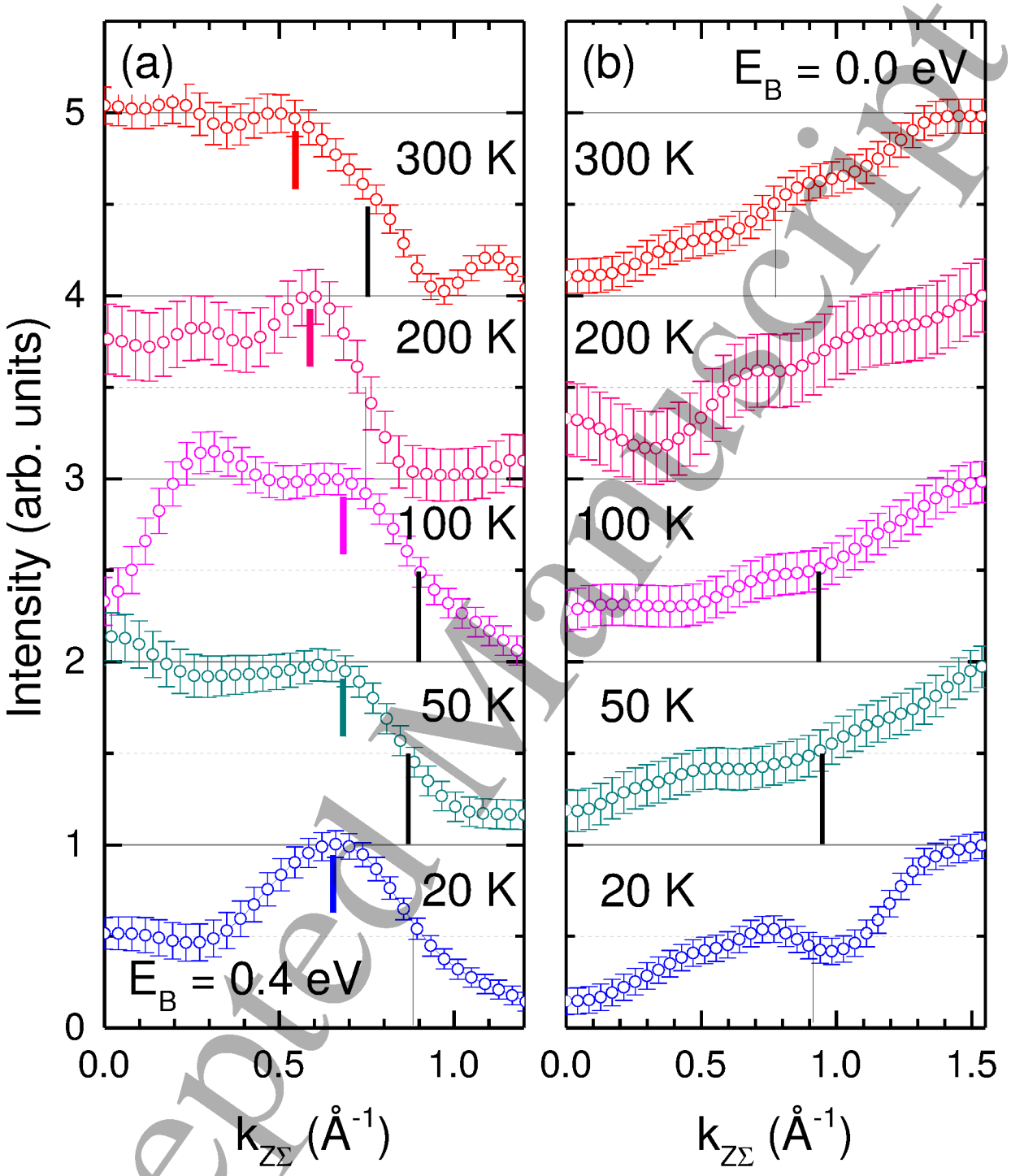

FIG. 5. (a,b) Momentum distribution curves along the Z - Σ direction $k_{Z\Sigma}$ at binding energies of 0.4 eV (a) and 0.0 eV (b) during slowly cooling the sample. The photoemission intensity $I_{\mathrm{N}}(E_B, k_x, k_y)$ has been normalized to the band D intensity maximum (a, colored mark), and to the intensity maximum at Γ (b), respectively. The distance of the trailing edge of band D from the Z point, $K_{Z\Sigma}$, is indicated at the half-maximum value, marked by a black line.

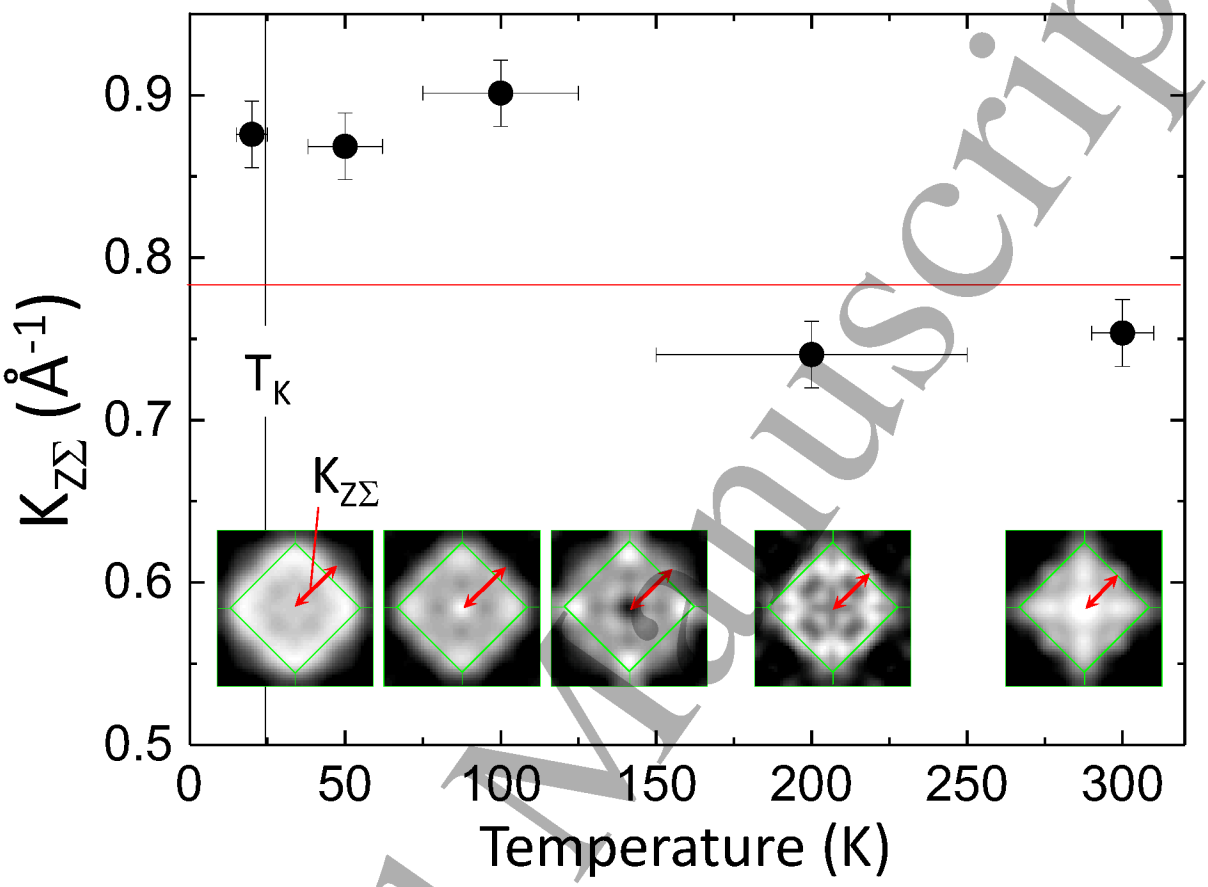

FIG. 6. Distance between the Z point and band D, $K_{Z\Sigma}$, along the Z-Σ symmetry line that crosses the Z-Y-Σ plane at a binding energy of 0.4 eV. The solid red line indicates the distance between Z and Σ. The data at intermediate temperatures were recorded during slow cooling. The horizontal bars indicate the range of temperatures during which the corresponding data were recorded. Constant energy maps for the corresponding temperatures are shown as insets (white means high intensity).

the statistical evidence for this difference is lower than for $E_B = 0.4$ eV. Note that the momentum at the half-maximum value of the photoemission intensity does not indicate the actual band position at E_F but rather reveals the temperature-induced change of the band position.

Based on the aforementioned observations we have chosen the D band dispersion at a binding energy of 0.4 eV as the most characteristic change The series of constant energy

maps at $E_B = 0.4$ eV, shown in Fig. 6, depicts the temperature-dependent behavior of band D. As a measure of the characteristic wave vector along the Z-Σ direction we determine the distance $K_{Z\Sigma}$ from the central Z point to the half maximum intensity at the trailing edge of the photoemission intensity [see Fig. 5(a)]. At 20 K this distance is significantly larger than the distance between the Z point and the Σ point, while at 300 K $K_{Z\Sigma}$ is close to $\overline{Z\Sigma}$, therefore indicating the decrease from the large to the small wave vector to occur between 100 K and 200 K. The characteristic temperature T^* for the change of the electronic structure is thus considerably larger than the Kondo temperature of this compound, i.e. $T^* > 4T_K$.

IV. DISCUSSION

Our experimental result of a continuous change of the electronic band dispersion at temperatures far above T_K indicates a crossover behavior in the $4f$-derived band dispersion when decreasing the temperature from room temperature to 100 K, instead of a more abrupt onset close to T_K. This finding is at odds with standard models of heavy fermion systems and must be discussed in relation to previously obtained experimental and theoretical results.

For $YbRh_2Si_2$ the resistivity maximum occurs at 100 K[17]. As pointed out in Ref.[33] crystal field effects may shift the resistivity maximum to higher temperatures above T_K. Therefore, one expects the change of the Fermi surface to take place below 100 K, where electron waves scattered from individual Kondo ions interfere coherently to form a narrow band of heavy electrons. While some models obtain a coherence temperature far below T_K[34], others discuss the existence of a further independent energy scale in addition to T_K[35].

The Kondo lattice models predict an abrupt change of the electronic structure with increasing temperature. Instead, the single impurity model reveals a Kondo resonance that gradually looses spectral weight and becomes broader with increasing temperature but does not vanish. Therefore, the resonance can be observed up to $T > 10\ T_K$[5,15].

Thermodynamic properties, revealed by specific heat and inelastic neutron scattering, suggest that the properties and energy scales of Kondo lattices and single ion Kondo systems are very similar to each other[3]. For the case of the analogous Kondo lattice $CeIrIn_5$ ($T_K = 28$ K[36]), dynamical mean-field theory calculations propose a continuous change of the Fermi surface between 10 and 80 K[11]. This prediction thus suggests that the Fermi surface change occurs considerably above T_K. To test this prediction in the case of $YbRh_2Si_2$, Kum-

mer et al.[15] have explicitly shown by ARPES that the Fermi surface remains temperature-independent in a wide temperature range between 1 and 100 K. This observation is inconsistent with the dynamical mean-field periodic Anderson model. Instead, a renormalized band structure approach[15] could explain the absence of changes of the Fermi surface up to 100 K. In the latter case the low temperature state is formed via a slow crossover similar to the single-impurity behavior and the large Fermi surface remains present until at least 100 K.

Our experimental result supports this theoretical prediction. In particular, we observe an indirect hint of the anticipated transition from localized to itinerant $4f$ states with decreasing temperature via the change of band positions. While the energy resolution of 155 meV in our experiment prohibits a direct observation of the band hybridization seen in Ref. 15, shifts of band D suggest the change of the Fermi surface to take place between 100 and 200 K.

While this finding is inconsistent with the prediction of the periodic Anderson model, it is in good agreement with the experimentally observed changes in core level spectra, resonant X-ray electron scattering[15] and scanning tunneling spectroscopy[18]. The temperature-dependent changes of the optical conductivity spectra[37] also indicate that band modulations occur at much higher temperature than T_K. Moreover, pronounced changes in optical conductivity are observed over a large energy scale of about 500 meV, consistent with our observations. Finally, our results agree with recent time-resolved ARPES experiments, where it was found that the $f-d$ hybridization decreases smoothly with increasing electronic temperature up to 250 K[19]. In fact, early systematic studies of carrier relaxation dynamics in a series of heavy fermions[38–41] and Kondo insulators[38,39,42,43] suggest the presence of a hybridization gap to temperatures far above their respective Kondo temperatures.

V. CONCLUSION

We investigated the temperature-dependent electronic band dispersion of the model Kondo lattice system $YbRh_2Si_2$ in the temperature range of 20 K to 300 K. Specific heat measurements[17] and inelastic neutron scattering data[44] indicate its prototypical Kondo heavy fermion behavior with a Kondo temperature of $T_K = 25$ K. The heavy fermion behavior has been attributed to the many-body electron correlation of the localized Yb $4f$ electrons with the itinerant conduction electrons. The question how this correlation changes the electronic

quasi particle states and in which temperature range this takes place, has been controversially discussed. From transport measurements and in accordance with the dynamical mean-field Anderson model one would expect that increasing temperature suppresses the correlation in a similar temperature range as the heavy fermion behavior vanishes. In contrast, a single impurity many-body model suggests a persistent electron correlation effect up to much higher temperatures. Using bulk-sensitive angular resolved photoemission spectroscopy in the hard X-ray regime, we demonstrate that the electronic structure of $YbRh_2Si_2$ changes with increasing temperature between 100 K and 200 K, i.e. far above the Kondo temperature $T_K = 25$ K of this Kondo lattice system. Our present study suggests that the Fermi surface change occurs at a much higher temperature than the loss of coherence. Therefore it seems that these two phenomena are not directly linked.

VI. ACKNOWLEDGEMENTS

Sincere thanks are due to A. Oelsner (Surface Concept GmbH) for continuous support. Funding by BMBF (projects 05K16UM1, 05K16UMC and 05K19UM1) and Deutsche Forschungsgemeinschaft (DFG, German Research Foundation) - TRR 173 – 268565370 and TRR288 – 422213477 (projects A03, B04, B08) is gratefully acknowledged.

---

* elmers@uni-mainz.de

[1] F. Steglich, J. Aarts, C. Bredl, W. Liecke, D. Meschede, W. Franz, and H. Schafer, Phys. Rev. Lett. **43**, 1892 (1979).

[2] A. A. Abrikosov, Physics **2**, 5 (1965).

[3] K. Andres, J. E. Graebner, and H. R. Ott, Phys. Rev. Lett. **35**, 1779 (1975).

[4] J. Allen, S.-J. Oh, M. B. Maple, and M. S. Torikachvili, Phys. Rev. B **28**, 5347 (1983).

[5] S. Seiro, L. Jiao, S. Kirchner, S. Hartmann, S. Friedemann, C. Krellner, C. Geibel, Q. Si, F. Steglich, and S. Wirth, Nature Comm. **9**, 3324 (2018).

[6] R. M. Martin, J. Appl. Phys. **53**, 2143 (1982).

[7] S. Nakamura, K. Hyodo, Y. Matsumoto, Y. Haga, H. Sato, S. Ueda, K. Mimura, K. Saiki, K. Iso, M. Yamashita, S. Kittaka, T. Sakakibara, and S. Ohara, J. Phys. Soc. Jap. **89**, 024705

(2020).

[8] S. Danzenbächer, D. Vyalikh, K. Kummer, C. Krellner, M. Holder, M. Höppner, Y. Kucherenko, C. Geibel, M. Shi, L. Patthey, S. Molodtsov, and C. Laubschat, Phys. Rev. Lett. **107**, 267601 (2011).

[9] M. Guettler, A. Generalov, S. Fujimori, I, K. Kummer, A. Chikina, S. Seiro, S. Danzenbaecher, Y. M. Koroteev, E. Chulkov, V, M. Radovic, M. Shi, N. C. Plumb, C. Laubschat, J. W. Allen, C. Krellner, C. Geibel, and D. V. Vyalikh, Nature Comm. **10**, 796 (2019).

[10] P. W. Anderson, Phys. Rev. **124**, 41 (1961).

[11] H. C. Choi, B. I. Min, J. H. Shim, K. Haule, and G. Kotliar, Phys. Rev. Lett **108**, 016402 (2012).

[12] D. V. Vyalikh, S. Danzenbächer, Y. Kucherenko, K. Kummer, C. Krellner, C. Geibel, M. G. Holder, T. K. Kim, C. Laubschat, M. Shi, L. Patthey, R. Follath, and S. L. Molodtsov, Phys. Rev. Lett. **105**, 237601 (2010).

[13] D. V. Vyalikh, S. Danzenbächer, A. N. Yaresko, M. Holder, Y. Kucherenko, C. Laubschat, C. Krellner, Z. Hossain, C. Geibel, M. Shi, L. Patthey, and S. L. Molodtsov, Phys. Rev. Lett. **100**, 056402 (2008).

[14] S. Danzenbächer, Y. Kucherenko, D. V. Vyalikh, M. Holder, C. Laubschat, A. N. Yaresko, C. Krellner, Z. Hossain, C. Geibel, X. J. Zhou, W. L. Yang, N. Mannella, Z. Hussain, Z.-X. Shen, M. Shi, L. Patthey, and S. L. Molodtsov, Phys. Rev. B **75**, 045109 (2007).

[15] K. Kummer, S. Patil, A. Chikina, M. Guettler, M. Hoeppner, A. Generalov, S. Danzenbächer, S. Seiro, A. Hannaske, C. Krellner, Y. Kucherenko, M. Shi, M. Radovic, E. Rienks, G. Zwicknagl, K. Matho, J. W. Allen, C. Laubschat, C. Geibel, and D. V. Vyalikh, Phys. Rev. X **5**, 011028 (2015).

[16] S. Kirchner, S. Paschen, Q. Chen, S. Wirth, D. Feng, J. D. Thompson, and Q. Si, Rev. Mod. Phys. **92**, 011002 (2020).

[17] O. Trovarelli, C. Geibel, S. Mederle, C. Langhammer, F. Grosche, P. Gegenwart, M. Lang, G. Sparn, and F. Steglich, Phys. Rev. Lett. **85**, 626 (2000).

[18] S. Ernst, S. Kirchner, C. Krellner, C. Geibel, G. Zwicknagl, F. Steglich, and S. Wirth, Nature **474**, 362 (2011).

[19] D. Leuenberger, J. A. Sobota, S. L. Yang, H. Pfau, D. J. Kim, S. K. Mo, Z. Fisk, P. S. Kirchmann, and Z. X. Shen, Phys. Rev. B **97**, 165108 (2018).

[20] D. Vasumathi, B. Barbiellini, A. A. Manuel, L. Hoffmann, T. Jarlborg, R. Modler, C. Geibel, F. Steglich, and M. Peter, Phys. Rev. B **55**, 11714 (1997).

[21] J. D. Denlinger, G.-H. Gweon, J. Allen, C. G. Olson, M. B. Maple, J. L. Sarrao, P. E. Armstrong, Z. Fisk, and H. Yamagami, J. Electron Spectrosc. Relat. Phenom. **117-118**, 347 (2001).

[22] A. Koitzsch, S. V. Borisenko, D. Inosov, J. Geck, V. B. Zabolotnyy, H. Shiozawa, M. Knupfer, J. Fink, B. Buchner, E. D. Bauer, J. L. Sarrao, and R. Follath, Phys. Rev. B **77**, 155128 (2008).

[23] A. Koizumi, G. Motoyama, Y. Kubo, T. Tanaka, M. Itou, and Y. Sakurai, Phys. Rev. Lett. **106**, 136401 (2011).

[24] Y. f. Yang, Z. Fisk, H.-O. Lee, J. D. Thompson, and D. Pines, Nature **454**, 611 (2008).

[25] A. X. Gray, J. Minar, S. Ueda, P. R. Stone, Y. Yamashita, J. Fujii, J. Braun, L. Plucinski, C. M. Schneider, G. Panaccione, H. Ebert, O. D. Dubon, K. Kobayashi, and C. S. Fadley, Nature Materials **11**, 957 (2012).

[26] S. Babenkov, K. Medjanik, D. Vasilyev, S. Chernov, C. Schlueter, A. Gloskovskii, Y. Matveyev, W. Drube, B. Schönhense, K. Rossnagel, H. J. Elmers, and G. Schönhense, Comm. Phys. **2**, 107 (2019).

[27] K. Medjanik, S. V. Babenkov, S. Chernov, D. Vasilyev, B. Schönhense, C. Schlueter, A. Gloskovskii, Y. Matveyev, W. Drube, H. J. Elmers, and G. Schönhense, J. Synchrotron Rad. **26**, 1996 (2019).

[28] K. Medjanik, O. Fedchenko, S. Chernov, D. Kutnyakhov, M. Ellguth, A. Oelsner, B. Schönhense, T. R. F. Peixoto, P. Lutz, C. H. Min, F. Reinert, S. Däster, Y. Acremann, J. Viefhaus, W. Wurth, H. J. Elmers, and G. Schönhense, Nature Materials **16**, 615 (2017).

[29] C. Krellner, S. Taube, T. Westerkamp, Z. Hossain, and C. Geibel, Phil. Mag. **92**, 2508 (2012).

[30] S. Ouardi, G. H. Fecher, and C. Felser, J. Electr. Spectr. Rel. Phen. **190**, 249 (2013).

[31] A. Regoutz, A. M. Ganose, L. Blumenthal, C. Schlueter, T.-L. Lee, G. Kieslich, A. K. Cheetham, G. Kerherve, Y.-S. Huang, R.-S. Chen, G. Vinai, T. Pincelli, G. Panaccione, K. H. L. Zhang, R. G. Egdell, J. Lischner, D. O. Scanlon, and D. J. Payne, Phys. Rev. Materials **3**, 025001 (2019).

[32] P. M. C. Rourke, A. McCollam, G. Lapertot, G. Knebel, J. Flouquet, and S. R. Julian, Phys. Rev. Lett. **101**, 237205 (2008).

[33] Y. Lassailly, A. K. Bhattacharjee, and B. Coqblin, Phys. Rev. B **31**, 7424 (1985).

[34] S. Sykora and K. Becker, Sci. Rep. **3**, 2691 (2013).

[35] C. Grenzebach, F. B. Anders, G. Czycholl, and T. Pruschke, Phys. Rev. B **74**, 195119 (2006).

[36] T. Willers, Z. Hu, N. Hollmann, P. O. Koerner, J. Gegner, T. Burnus, H. Fujiwara, A. Tanaka, D. Schmitz, H. H. Hsieh, H. J. Lin, C. T. Chen, E. D. Bauer, J. L. Sarrao, E. Goremychkin, M. Koza, L. H. Tjeng, and A. Severing, Phys. Rev. B **81**, 195114 (2010).

[37] S. Kimura, J. Sichelschmidt, J. Ferstl, C. Krellner, C. Geibel, and F. Steglich, Phys. Rev. B **74**, 132408 (2006).

[38] J. Demsar, V. Thorsmolle, J. Sarrao, and A. Taylor, Phys. Rev. Lett. **96**, 037401 (2006).

[39] J. Demsar, J. L. Sarrao, and A. J. Taylor, J. Phys. Condens. Matter **18**, R281 (2006).

[40] J. Demsar, V. V. Kabanov, A. S. Alexandrov, H. J. Lee, E. D. Bauer, J. L. Sarrao, and A. J. Taylor, Phys. Rev. B **80**, 085121 (2009).

[41] E. E. M. Chia, J.-X. Zhu, D. Talbayev, H. J. Lee, N. Hur, N. O. Moreno, R. D. Averitt, J. L. Sarrao, and A. J. Taylor, Phys. Rev. B **84**, 174412 (2011).

[42] M. Okawa, Y. Ishida, M. Takahashi, T. Shimada, F. Iga, T. Takabatake, T. Saitoh, and S. Shin, Phys. Rev. B **92**, 161108 (2015).

[43] J. Zhang, J. Yong, I. Takeuchi, R. L. Greene, and R. D. Averitt, Phys. Rev. B **97**, 155119 (2018).

[44] O. Stockert, M. M. Koza, J. Ferstl, C. Geibel, and F. Steglich, Sci. Techn. Adv. Mat. **8**, 371 (2007).